HHS Public Access

Author manuscript

J Am Chem Soc. Author manuscript; available in PMC 2018 November 08.

Published in final edited form as:

J Am Chem Soc. 2017 November 08; 139(44): 15560–15563. doi:10.1021/jacs.7b05960.

Targeting Unoccupied Surfaces on Protein–Protein Interfaces

David Rooklin[†,‡], **Ashley E. Modell**[†,‡], **Haotian Li**[†], **Viktoriya Berdan**[†], **Paramjit S. Arora**[*,†], and **Yingkai Zhang**[*,†,⊥]

[†]Department of Chemistry, New York University, New York, New York 10003, United States

[⊥]NYU-ECNU Center for Computational Chemistry, New York University–Shanghai, Shanghai 200122, China

Abstract

The use of peptidomimetic scaffolds to target protein–protein interfaces is a promising strategy for inhibitor design. The strategy relies on mimicry of protein motifs that exhibit a concentration of native hot spot residues. To address this constraint, we present a pocket-centric computational design strategy guided by AlphaSpace to identify high-quality pockets near the peptidomimetic motif that are both targetable and unoccupied. Alpha-clusters serve as a spatial representation of pocket space and are used to guide the selection of natural and non-natural amino acid mutations to design inhibitors that optimize pocket occupation across the interface. We tested the strategy against a challenging protein–protein interaction target, KIX/MLL, by optimizing a single helical motif within MLL to compete against the full-length wild-type MLL sequence. Molecular dynamics simulation and experimental fluorescence polarization assays are used to verify the efficacy of the optimized peptide sequence.

Mimicry of interfacial protein domains offers a promising strategy to rationally design inhibitors of protein–protein interactions (PPIs).[1–3] This strategy focuses on interfaces where a subset of the interacting residues from an endogenous PPI reside on a folded region.[4–7] The central goal of peptidomimetic design is to capture adequate binding energy on a small to medium sized cell permeable synthetic scaffold;[8–10] smaller sized mimics are easier to access if the binding epitopes can be localized to organized secondary or tertiary structure motifs rather than complex folds.[11] The classical approach for identifying residues that contribute significantly to binding, or “hot spot” residues, utilizes alanine scanning mutagenesis.[12,13] Though the overall approach of mimicking hot spots has yielded potent inhibitors for many protein complexes,[1] the general protein mimicry strategy is limited

[*]**Corresponding Authors**: arora@nyu.edu; yingkai.zhang@nyu.edu.

[‡]**Author Contributions**

D.R. and A.E.M. contributed equally.

ORCID

Paramjit S. Arora: 0000-0001-5315-401X

Yingkai Zhang: 0000-0002-4984-3354

Notes

The authors declare no competing financial interest.

Supporting Information

The Supporting Information is available free of charge on the ACS Publications website at DOI: 10.1021/jacs.7b05960.

Details of the computational protocol, peptide synthesis, purification and characterization, and binding assays (PDF)

because many PPI interfaces do not naturally exhibit a concentration of critical “hot spot” residues within a single, conveniently mimicked motif. Furthermore, the existing native hot spot residues may not optimally engage the target surface. To address these significant limitations to rational design of PPI inhibitors, we present a computational strategy to characterize the local interface structure at high resolution and enhance the interactions derived from a wild-type motif.

Our computational approach, termed AlphaSpace,[14] provides fragment-centric topographical mapping of protein surface structure to reveal new targetable pockets as well as underutilized subpocket space.[15–18] To rigorously establish the potential of AlphaSpace for interface analysis, we applied the algorithm to design sequences against a challenging PPI target that lacks the critical concentration of hot spot residues at a single helical interface. The KIX/MLL PPI interface represents a compelling test case for prospective, pocket-guided optimization of a helical peptide mimic because the hot spot residues of MLL are distributed between a strand region and a helical region (Figure 1). Furthermore, it has proven challenging to develop high affinity ligands for KIX using structure-based and screening approaches.[19–23]

The KIX domain of transcriptional coactivators CBP and p300 functions through two PPI docking sites where KIX can bind transactivation domains (TADs) from a variety of transcription factors.[24,25] KIX is a relatively flexible helical domain with a hydrophobic core that serves as an allosteric network of residues to transduce signal between the two PPI faces on opposing sides of the protein.[26] Aberrant interactions between KIX and oncogenic transcription factors have been associated with a variety of leukemias.[27] Inhibition of KIX/MLL has been hypothesized as a potential therapeutic strategy to down regulate the associated aberrant gene transcription. Because MLL employs a helical motif at the PPI interface, a helical mimetic may serve as starting point for inhibitor design. However, when the native peptide is truncated to contain just the helical segment, we experimentally observe that its interaction with KIX is abolished, demonstrating that hot spot residues that fall outside of MLL’s helical motif contribute critically to binding. We hypothesized that rational optimization of the helical motif to recover the binding affinity to within the range of the wild-type MLL will serve as a proof-of-concept study for AlphaSpace-guided design, as well as for future development of helix mimics as inhibitors of KIX and MLL complex formation.

We began by analyzing 40 PPI interfaces from NMR structures of both the KIX/MLL dimer (PDB: 2LXS) and the c-Myb/KIX/MLL trimer (PDB: 2AGH)[24,26] complexes using AlphaSpace.[14] Our analysis revealed two distinct pocket states, as noted previously,[24] and as illustrated in Figure 2, with high scoring pockets colored in green. Details are included in the Supporting Information. MLL$^{840–858}$ (DCGNILPS-DIMDFVLKNTP) adopts a β-strand conformation from the N-terminus to P^{846} and adopts a helical structure from S^{847}-T^{857}. *Pocket State 1* (observed in PDB: 2LXS, Figure 2A,C) represents the KIX/MLL dimer state; the primary high-scoring pocket-contact residue is within the N-terminal strand (L^{845}) and three moderate-scoring pocket-contact residues are identified within the helix (M^{850}, F^{852}, L^{854}). *Pocket State 2* (observed in PDB: 2AGH, Figure 2B,D) represents the c-Myb/KIX/MLL trimer state; the contribution to binding is calculated to be more evenly

distributed across 5 residues spanning both the strand (I^{844}, L^{845}) and the helix regions (F^{852}, V^{853}, T^{857}). Importantly, two critical optimization opportunities were observed exclusively for the trimer *Pocket State 2.* First, the side chain of M^{850} (helix) makes no direct contact with the KIX surface, but, if extended with a longer side chain, is positioned to extend into pocket 3 of *Pocket State 2*, which otherwise would be unoccupied by the truncation of L^{845}. Second, we observe the formation of an underutilized high-scoring pocket 2 near the C-terminus of the helical motif, proximal to residue T^{857}.

With the selection of *Pocket State 2*, which is more amenable to optimization due to the identification of high-scoring underutilized pocket space adjacent to the helical motif, we then employed alpha-cluster, a novel feature introduced in AlphaSpace, as a physical representation of targetable pocket space to guide the selection of mutations able to enhance pocket-ligand complementarity across the interface, as illustrated in Figure 3. We considered natural and non-natural amino acids, using rotamer states taken from the SwissSidehain database,[28] to identify residues with the capacity to extend directly into underutilized pocket space (i.e., to achieve shape complementarity with the alpha-cluster representation of each pocket respectively) while avoiding steric overlap with the pocket lining atoms in KIX. In total, we selected 4 mutations (2 natural and 2 non-natural) to enhance pocket occupation across the selected conformation from *Pocket State 2* (Figure 3B,D,F,H): M^{850} > Bcs (benzyl-cysteine), F^{852} > 2mf (2-methyl-phenylalanine), V^{853} > Ile, and T^{857} > Tyr. Additionally, we incorporated a potential electrostatic interaction near Pocket 2 by substituting a carboxylate for the amide at the C-terminus of the peptide, similar to previous studies that interrogated the highly positively charged C-terminus of KIX.[25,29]

We experimentally evaluated the computational predictions in a series of six 12-residue peptides, starting with the truncated wild-type (WT) helix S^{847}-P^{858} (MLL1) and cumulatively introducing mutations in the following order: Bcs^{850} (MLL2), Y^{857} (MLL3), I^{853} (MLL4), COO^{-} (MLL5), $2mf^{852}$ (MLL6). We obtained direct and competitive binding constants for these sequences against KIX (Table 1). Results reflect our prediction that Bcs^{850} and Y^{857} are key modifications that introduce novel high-scoring interactions. These two mutations alone recover much of the binding affinity lost in the truncation of the peptide. The remaining mutations each enhance affinity incrementally, leading to the optimized sequence, MLL6, which exhibits binding affinity similar to that of the WT sequence. Circular dichroism spectroscopy suggests that the conformations of the modified peptides do not deviate from that of MLL1 (Figure S7).

Our next task was to employ extensive explicit-solvent molecular dynamics simulations to characterize and compare the binding mechanism between KIX and three peptides: full-length wild-type peptide MLL-WT, truncated MLL1, and our designed MLL6. For each KIX–peptide complex, we performed five 300 ns production MD simulations using Amber14, and analyzed using AlphaSpace (see SI for details). Starting structures for the simulations were initialized from PDB: 2AGH.1 (with c-Myb removed) in order to evaluate and compare the predicted interactions against *Pocket State* 2. The simulations reinforce that the full-length wild-type MLL relies heavily on the N-terminus strand residues I^{844} and L^{845} to achieve a high degree of pocket occupation (Figure S2). The truncated wild-type peptide (MLL1) recovers some of the lost pocket occupation through M^{850} (Figure S3), but the

overall pocket occupation is greatly reduced, and the instability of the complex can be visualized in the large spatial variation in the average position of each residue-occupied pocket space between the five independent simulations (Figure S4). Simulations of the optimized helical motif (MLL6), on the other hand, reveal a consistent stable binding mode in four out of the five independent simulations, which exhibit very low spatial fluctuation in the average positions of the residue-occupied pockets (Figure S4). All four of the optimized residues exhibit enhancements to average pocket occupation compared to their respective values from the full-length wild-type MLL simulation (Figure S2). Significantly, modeling MLL6 recapitulated the high scoring pockets from *Pocket State 2* (Figure S5).

Finally, to examine our computational characterization of KIX/MLL6 binding interface, we performed experimental alanine scanning for the four optimized residues within MLL6, data listed in Table 2. Competitive binding to KIX is abolished or nearly abolished with each of the alanine mutations, indicating that all four designed residues (Bcs^{850}, $2mf^{852}$, I^{853}, Y^{857}) have become hot spot residues that are responsible for achieving the observed KIX/MLL6 affinity. These experimental mutational results are consistent with our computational findings and further corroborate our proposed pocket-centric design strategy. We also tested the significance of the carboxylate at the C-terminus by amide substitution, but binding was not significantly affected.

In summary, a detailed pocket-centric characterization of the target KIX/MLL interface facilitated the identification of a well-defined bimodal binding mechanism and allowed us to select the more conducive pocket state for optimization of ligand. AlphaSpace was used to detect and evaluate underutilized targetable pocket space and to directly guide the selection of mutations predicted to enhance overall pocket occupation at the interface. The proposed optimized peptide successfully recovers the majority of the binding affinity lost in the truncation of the full length MLL (1.0 ± 0.3 μM) to the isolated helical motif (>100 μM), bringing direct binding back into the low micromolar range (3.3 ± 0.5 μM) with our optimized inhibitor MLL6. We postulate this general pocket-centric approach to peptide optimization can be applied to support the extensibility of the peptidomimetic strategy for PPI inhibition.

Supplementary Material

Refer to Web version on PubMed Central for supplementary material.

Acknowledgments

We thank the National Institutes of Health (R01GM073943 and R01GM120736) for financial support of this work. A.E.M. is supported by the Margaret and Herman Sokol Fellowship.

References

1. Pelay-Gimeno M, Glas A, Koch O, Grossmann TN. Angew Chem, Int Ed. 2015; 54:8896.
2. Sawyer N, Watkins AM, Arora PS. Acc Chem Res. 2017; 50:1313. [PubMed: 28561588]
3. Sheng C, Dong G, Miao Z, Zhang W, Wang W. Chem Soc Rev. 2015; 44:8238. [PubMed: 26248294]
4. Wells JA, McClendon CL. Nature. 2007; 450:1001. [PubMed: 18075579]

5. Jochim AL, Arora PS. ACS Chem Biol. 2010; 5:919. [PubMed: 20712375]
6. Watkins AM, Arora PS. ACS Chem Biol. 2014; 9:1747. [PubMed: 24870802]
7. London N, Raveh B, Schueler-Furman O. Curr Opin Chem Biol. 2013; 17:952. [PubMed: 24183815]
8. Checco JW, Kreitler DF, Thomas NC, Belair DG, Rettko NJ, Murphy WL, Forest KT, Gellman SH. Proc Natl Acad Sci USA. 2015; 112:4552. [PubMed: 25825775]
9. Lao BB, Drew K, Guarracino DA, Brewer TF, Heindel DW, Bonneau R, Arora PS. J Am Chem Soc. 2014; 136:7877. [PubMed: 24972345]
10. Cummings CG, Hamilton AD. Curr Opin Chem Biol. 2010; 14:341. [PubMed: 20430687]
11. Arkin MR, Tang Y, Wells JA. Chem Biol. 2014; 21:1102. [PubMed: 25237857]
12. Kortemme T, Kim DE, Baker D. Sci Signaling. 2004; 2004:pl2.
13. Massova I, Kollman PA. J Am Chem Soc. 1999; 121:8133.
14. Rooklin DW, Wang C, Katigbak J, Arora PS, Zhang Y. J Chem Inf Model. 2015; 55:1585–1599. [PubMed: 26225450]
15. Brenke R, Kozakov D, Chuang GY, Beglov D, Hall D, Landon MR, Mattos C, Vajda S. Bioinformatics. 2009; 25:621. [PubMed: 19176554]
16. Fuller JC, Burgoyne NJ, Jackson RM. Drug Discovery Today. 2009; 14:155. [PubMed: 19041415]
17. Volkamer A, Griewel A, Grombacher T, Rarey M. J Chem Inf Model. 2010; 50:2041. [PubMed: 20945875]
18. Guvench O, MacKerell AD Jr. PLoS Comput Biol. 2009; 5:e1000435. [PubMed: 19593374]
19. Bates CA, Pomerantz WC, Mapp AK. Biopolymers. 2011; 95:17. [PubMed: 20882601]
20. Majmudar CY, Højfeldt JW, Arevang CJ, Pomerantz WC, Gagnon JK, Schultz PJ, Cesa LC, Doss CH, Rowe SP, Vásquez V, Tamayo-Castillo G, Cierpicki T, Brooks CL, Sherman DH, Mapp AK. Angew Chem, Int Ed. 2012; 51:11258.
21. Frangioni JV, LaRiccia LM, Cantley LC, Montminy MR. Nat Biotechnol. 2000; 18:1080. [PubMed: 11017047]
22. Volkman HM, Rutledge SE, Schepartz A. J Am Chem Soc. 2005; 127:4649. [PubMed: 15796530]
23. Li BX, Xiao X. ChemBioChem. 2009; 10:2721. [PubMed: 19810079]
24. De Guzman RN, Goto NK, Dyson HJ, Wright PE. J Mol Biol. 2006; 355:1005. [PubMed: 16253272]
25. Thakur JK, Yadav A, Yadav G. Nucleic Acids Res. 2014; 42:2112. [PubMed: 24253305]
26. Brüschweiler S, Konrat R, Tollinger M. ACS Chem Biol. 2013; 8:1600. [PubMed: 23651431]
27. Denis CM, Chitayat S, Plevin MJ, Wang F, Thompson P, Liu S, Spencer HL, Ikura M, LeBrun DP, Smith SP. Blood. 2012; 120:3968. [PubMed: 22972988]
28. Gfeller D, Michielin O, Zoete V. Nucleic Acids Res. 2013; 41:D327. [PubMed: 23104376]
29. Radhakrishnan I, Perez-Alvarado GC, Parker D, Dyson HJ, Montminy MR, Wright PE. J Mol Biol. 1999; 287:859. [PubMed: 10222196]

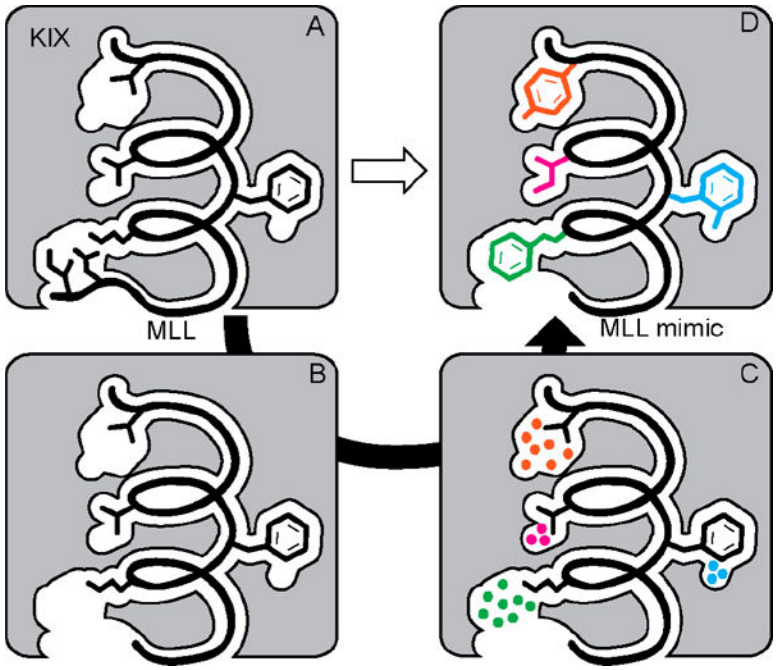

Figure 1.

Pocket-centric rational design to target a recalcitrant protein–protein interface. Overview of study: (A) MLL, the natural binding partner of coactivator KIX, utilizes residues on a contiguous helix-strand motif to bind KIX. (B) Individually, the helical segment does not encompass sufficient binding energy to bind KIX with high affinity. (C and D) Detection of underutilized pocket space on KIX using AlphaSpace allows design of a modified MLL peptide containing natural and non-natural amino acids for optimal interactions.

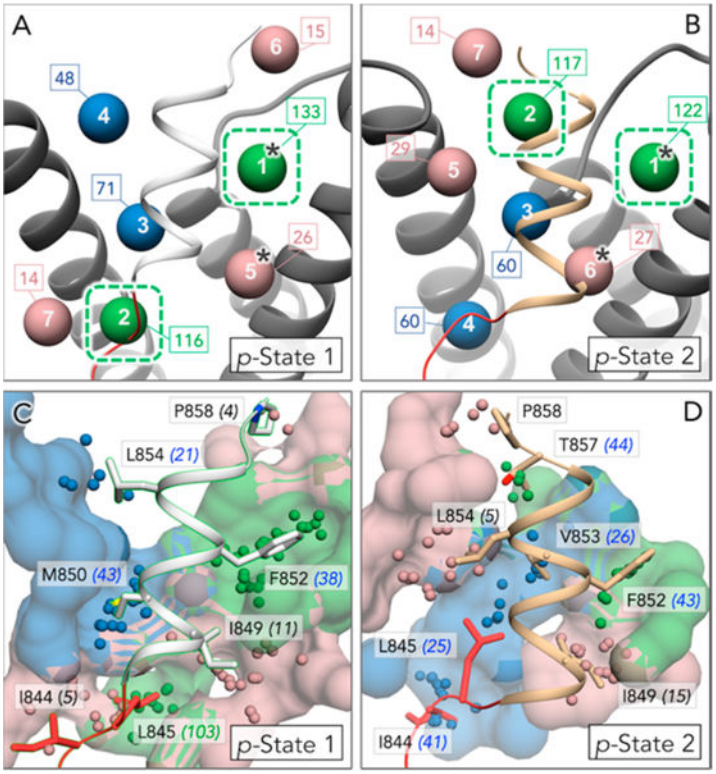

Figure 2.

Two pocket states at the KIX/MLL interfaces revealed by AlphaSpace analysis are illustrated in panels A and B: green, blue, pink spheres refer to high, medium and low scoring pockets, respectively. Pockets are ranked and numbered by their average nonpolar pocket volume with #1 having the highest pocket score. Asterisks denote pockets with atomic composition conserved between the two pocket states. KIX is represented as a dark gray ribbon and MLL is represented as light gray ribbon (A, C) or tan ribbon (B, D). Analyzed average pocket occupation by MLL residue is shown in panels C and D with representative structures from *Pocket State 1* and *Pocket State 2*. The representative sets of pocket atoms and alpha-clusters are colored by average score as in panels A and B. Residues outside the helical motif are highlighted in red. C-Myb from *Pocket State 2* is not shown for clarity.

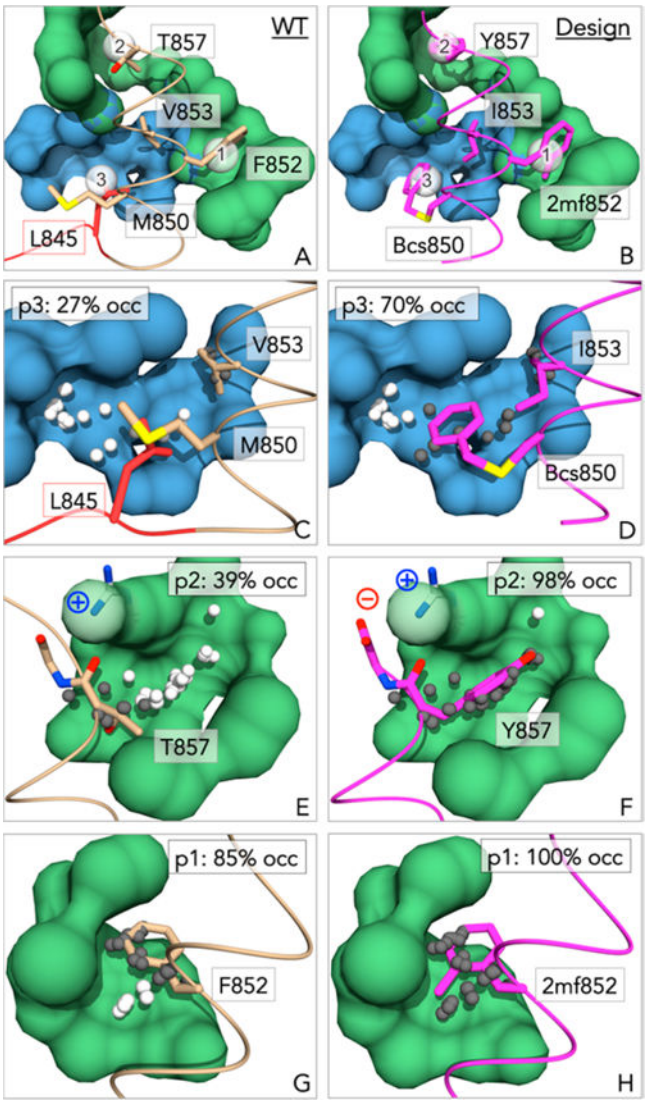

Figure 3.

Localized optimization of pocket-residue complementarity is illustrated with the wild-type sequence on the left and the designed sequence on the right for a selected conformation from *Pocket State 2*: PDB: 2AGH.1. Panels A and B show an overview of the 3 pockets being optimized. Panels (C,D), (E,F), and (G,H) illustrate the optimizations for pocket 3, pocket 2, and pocket 1 respectively. Unoccupied alpha-atoms are highlighted in white; occupied alpha-atoms are colored dark gray. Percentage pocket occupation is listed for each panel, indicating the enhancements achieved in the optimization.

Table 1

Direct and Competitive Binding Data for the Wild-Type and Optimized MLL Sequences Targeting KIX [*]

MLL	Sequence[a]	K_d,[b](μM)	K_i[c](μM)
WT	X-DCGNILPSDIMDFVLKNTP	1.0±0.3	3.0±0.8
1	X-SDIMDFVLKNTP-NH2	>100	>1000
2	X-SDI C* DFVLKNTP-NH_2	>15	>500
3	X-SDI C* DFVLKN Y P-NH_2	8.3±1.3	58±35
4	X-SDI C* DF I LKN Y P-NH_2	7.3±1.5	32±19
5	X-SDI C* DF I LKN Y P- OH	6.0±0.8	24±15
6	X-SDI C* D F* I LKN Y P- OH	3.3±0.5	22 ±8

[*] X = Flu-βAlanine- for direct binding experiments or Ac- for competition experiments.

[a] The wild-type (WT) sequence is amidated at the C-terminus. Underlined residues denote hot spot residues; highlighted residues are positions that were modified during the design process. C* = benzyl-cysteine, F* = 2-methyl-phenylalanine.

[b] Direct binding of the fluorescein-conjugated peptides, assessed using a fluorescence polarization assay.

[c] Competitive inhibition against fluorescently labeled wild-type peptide, analyzed using a polarization assay.

Table 2

Mutagenesis of the Optimized Sequence Reveals Important Contacts

MLL	Sequence	K_i[a]
6	Ac-SDI C * D F * I LKN Y P- OH	22 ± 8
C*→A	Ac-SDI A D F * I LKN Y P- OH	NB
F*→A	Ac-SDI C * D A I LKN Y P- OH	>500
I→A	Ac-SDI C * D F * A LKN Y P- OH	>500
Y→A	Ac-SDI C * D F * I LKN A P- OH	NB
OH→NH_2	Ac-SDI C * D F * I LKN Y P- NH 2	20±26

[a]Competitive inhibition against fluorescently labeled wild-type peptide, analyzed using a fluorescence polarization assay. Highlighted residues are positions that were modified.